Spontaneous Emission inside a Hyperbolic Metamaterial Waveguide

Diane J. Roth,*,[†] Alexey V. Krasavin,[†] Alexander Wade,[†] Wayne Dickson,[†] Antony Murphy,[‡]
Stéphane Kéna-Cohen,[§] Robert Pollard,[‡] Gregory A. Wurtz,[†,∥] David Richards,[†] Stefan A. Maier,[⊥]
and Anatoly V. Zayats[†]

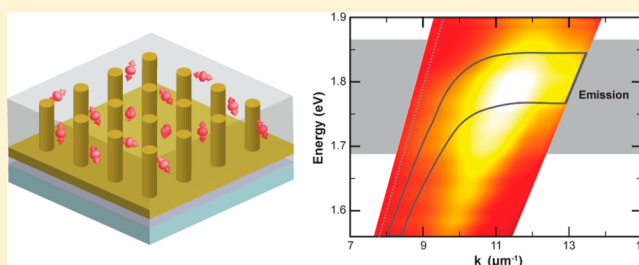[†]Department of Physics, King's College London, Strand, London, WC2R 2LS, United Kingdom
[⊥]Blackett Laboratory, Department of Physics, Imperial College London, London SW7 2AZ, United Kingdom
[‡]Centre for Nanostructured Media, The Queen's University of Belfast, Belfast BT7 1NN, United Kingdom
[§]Department of Engineering Physics, École Polytechnique de Montréal, Montréal, Quebec Canada

ABSTRACT: The ability to control the rate of spontaneous emission via the design of nanostructured materials with appropriate electromagnetic properties is important in the development of novel fast sources of incoherent illumination, single photon emitters for quantum optical applications, laser physics, and de-excitation of electronic states leading to photodegradation in organic materials. Here, for an emitter placed inside a hyperbolic metamaterial slab of finite thickness comprised of an array of gold nanorods, we experimentally demonstrate an enhancement of the fluorescence coupled to
the waveguided plasmon-polariton modes of the metamaterial. We show that fluorescence properties in such a finite-size metamaterial design behave differently from commonly studied infinite metamaterials or when the emitters are placed near the metamaterial interface. The emitters inside the metamaterial waveguide exhibit an almost 50-fold reduction of their lifetime, whereas a much smaller reduction (a factor of 2−3) is observed for emitters placed on top of the metamaterial. While in both cases the emission from the metamaterial can be radiated in the far field (up to 18% of the total emitted intensity, depending on the emitter position with respect to the nanorods), the coupling to waveguided modes of the metamaterial slab provides an efficient means to shape the emission spectrum for each polarization. The considered geometry is ideal for designing integrated, fast optical sources for data communications, sensing, or quantum photonic applications.

KEYWORDS: hyperbolic metamaterials, plasmonic nanorods, spontaneous emission, Purcell effect, waveguides

Controlling the spontaneous emission of fluorescent emitters is of great interest for a wide range of applications ranging from biosensing and imaging, where the aim is to favorably modify the spectral properties of emitters in order to increase detection sensitivity, to quantum information processing, where the use of efficient single photon sources is needed. The Purcell effect,[1] which describes the modification of the spontaneous emission lifetime, has been investigated in many different material environments where the local density of electromagnetic states (LDOS), $\rho(\omega,r)$, is modified at a frequency ω and a position r of the emitter. This determines the spontaneous emission rate $\Gamma(\omega) \sim \rho(\omega,r)$.[2,3] In particular, structures such as photonic crystal cavities,[4,5] micropillar resonators,[6,7] plasmonic films, nanoparticles[8,9] and waveguiding nanostructures[10] have been the subject of numerous studies in this context.

Hyperbolic metamaterials,[11,12] with their specific isofrequency surfaces, have recently emerged at the forefront of the Purcell factor design.[13] These strongly anisotropic metamaterials can be described by an effective permittivity tensor having the real part of the diagonal components of opposite signs. In contrast with isotropic materials or anisotropic metamaterials operating in the elliptic regime of

dispersion, hyperbolic metamaterials exhibit open isofrequency surfaces. This leads to the presence of high wavevectors of supported electromagnetic modes and high density of electromagnetic states, to which the radiation of an excited emitter can couple, dramatically influencing the process of spontaneous emission.

Hyperbolic metamaterials can either be realized as metal-dielectric multilayers,[14] aligned nanorod assemblies,[15,16] or natural van der Waals bonded polar materials.[17] To date, several experimental studies involving hyperbolic metamaterials that incorporate dye-doped dielectric layers,[18−20] emitters on multilayers,[21] or nanorod-based metamaterials,[22] as well as theoretical studies of emitters near[23,24] or inside[25,26] the metamaterial, particularly revealing the presence of a self-induced torque acting on the emitter,[27] have been reported. The inexpensive, straightforward, and scalable fabrication of nanorod-based hyperbolic metamaterials using a self-assembled approach[28] combined with the ability to tune their geometrical properties (diameter, length, and material of the nanorods as well as separation between) allow their electromagnetic

properties to be tailored in a wide spectral range. This geometry also provides significant advantages with regard to incorporating molecular emitters inside the metamaterial.

While most of the previous studies were focused on the effect of the material environment on free-space-radiated emission, in many applications, it is guided light that is important to provide the capability for photonic integration of such novel light sources, for example, single-photon light sources. The previous experimental and theoretical studies are dominantly limited to "bulk" metamaterials, that is, "infinitely" thick, so that no significant interaction between the slab boundaries occurs due to propagation losses, and effects related to waveguided or cavity modes are either not present or suppressed. In this paper, we experimentally investigate the spontaneous emission of various dyes inside a metamaterial-based planar waveguide of finite thickness.[29] It is shown that the structure of the guided modes plays a significant role in determining the spontaneous emission properties. The spectrum and lifetime of the emission can be controlled separately for TM and TE polarizations by coupling to different modes of the waveguide.

■ RESULTS AND DISCUSSION

Mode Structure of the Metamaterial Waveguide. The metamaterial studied here consists of an array of gold nanorods (approximately 38 nm in diameter, 150 nm in length, with 80 nm spacing) embedded in a dye-doped PMMA matrix (see Methods section for the details of the fabrication). The anisotropic behavior of this type of metamaterial can be described within a local effective medium theory (EMT) using the Maxwell-Garnett approximation (see Methods section). The extinction spectra of the metamaterial are typical of nanorod-based metamaterials with the presence of an epsilon-near-zero (ENZ) range around the effective plasma frequency of the metamaterial (2.08 eV in this instance, corresponding to 596 nm wavelength) which is the onset of the hyperbolic dispersion regime (Figure 1a,b). Several different organic dyes were used to study the modification of spontaneous emission properties with the emission wavelengths spanning the elliptic (ε_x, $\varepsilon_z > 0$) as well as the hyperbolic ($\varepsilon_x > 0 > \varepsilon_z$) dispersion regime of the metamaterial (Figures 1a and 2a).

The metamaterial slab, with the parameters considered in this study and in the spectral range of interest, acts as a waveguide for bulk plasmon-polariton modes.[29] This is evidenced by the experimental and modeled dispersions for TM-polarized waves, with an electric field component along the extraordinary axis of the anisotropic metamaterial, also corresponding to the nanorod axis or z-axis in Figure 1a (Figure 2a,b). In the same wavelength range, the slab also supports a single conventional TE mode (with the electric field normal to the nanorods), similar to transparent dielectric waveguides since it is only affected by the $\varepsilon_x = \varepsilon_y > 0$ components of the effective permittivity tensor of the metamaterial slab (Figure 2c,d). These modes, located between the light-lines of the substrate and superstrate, can be accessed in total internal reflection using a prism coupler matched to the refractive index of the substrate.[15] Higher order TM modes, situated closer to the effective plasma frequency of the metamaterial (see Figure 2, caption), are not identifiable in the reflection spectra due to high ohmic losses of gold in this spectral range. The strong spectral overlap between the TM1 mode of the metamaterial slab and the emission spectrum of the bare LD700 dye (Figures 2 and 3), can lead to a significant coupling of the emitted light into this mode. However, as the
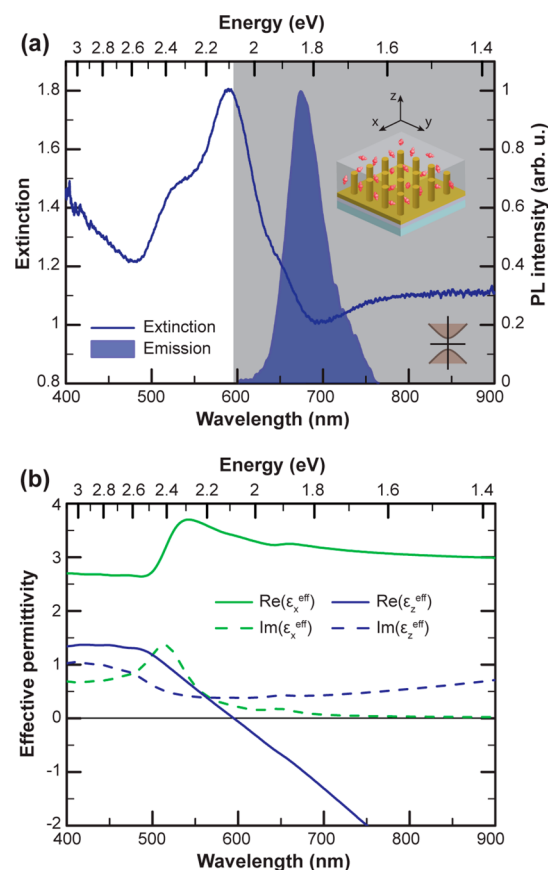

Figure 1. Optical properties of the metamaterial and fluorescence lifetime analysis. (a) Experimental extinction spectrum ($-\log T$) of the nanorod metamaterial hybridized with polymer containing LD700 dye measured at 40° angle of incidence and the emission spectra LD700 dye in the polymer on a glass substrate. Inset: schematics of the nanorod metamaterial. The hyperbolic dispersion range is shown in gray. (b) Spectra of real (Re) and imaginary (Im) parts of the principal components of the effective permittivity tensor of the metamaterial in (a). Orientation of the coordinate axes is shown in the inset of (a).

result of the random orientation of the molecules in the matrix, the emission can also couple to TE modes. The coupling to the different modes can be discriminated using a polarization analysis of the leakage radiation (see Methods section).

Photoluminescence Coupled to the Metamaterial Mode. The measured angular dispersion of the TM-polarized photoluminescence follows the dispersion of the TM wave-guided mode (Figure 3a), indicating that the emission is predominantly coupled into this mode. A 2.5× stronger PL intensity coupled to the mode is observed with regard to the emission scattered directly into free space, despite the additional losses associated with the waveguiding of bulk plasmon-polaritons in the metamaterial slab. A significant red-shift of the emission maximum is also observed with respect to the emission of LD700 in a bare polymer matrix (without the metamaterial; Figure 3b). This shift is consistent with the dispersion profile of the guided mode and is determined by the overlap of the density of photonic states associated with the mode, the dipolar emission spectrum of the fluorophores inside the metamaterial layer, and their spatial distribution inside the nanorod array. Even higher emission enhancements can in principle be achieved by further adjusting the waveguide dispersion to the emission spectrum of the fluorophores, which can be done by carefully varying the thickness of the
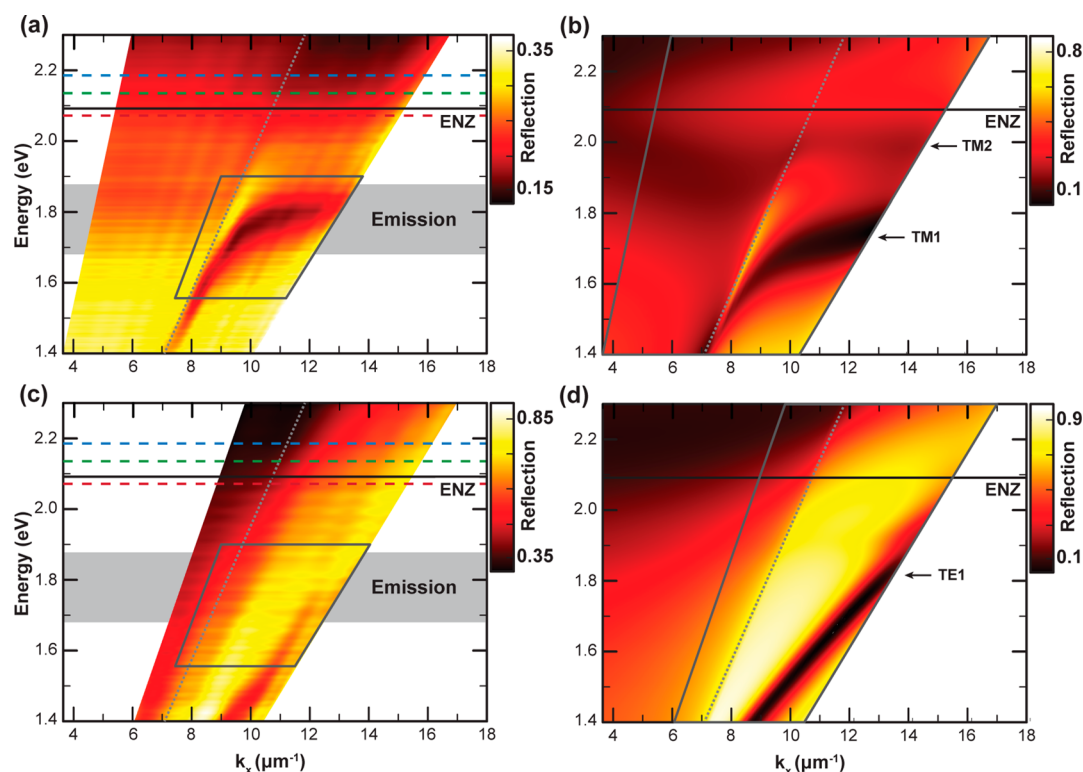
Figure 2. Mode structure of metamaterial slab. Reflection dispersions of the metamaterial slab waveguide for (a, b) TM and (c, d) TE polarizations: (a, c) Experiment and (b, d) analytical modeling using the transfer matrix method and an effective medium theory. The position of the effective plasma frequency of the metamaterial (solid horizontal line), the light line in air (gray dotted line), the emission band of LD700 dye (greyed region), and the peak emission wavelengths of the other studied dyes (dashed lines: blue, R590; green, R610; and red, R640) are shown.

metamaterial waveguide. Similarly to the TM-polarized PL, the TE-polarized PL follows the dispersion of the TE waveguided mode. The intensity increase is however lower than for the TM-polarized waveguided emission (Figure 3c,d). It should be noted that the high relative intensity increase in Figure 3c can be seen at the wavelengths away from the emission peak in the polymer matrix, which corresponds to the wavelength range where the overall PL intensity is very low (Figure 3d), causing a high relative enhancement.

Time-Resolved Photoluminescence. The time-resolved photoluminescence of several emitters with PL emission inside and outside the wavelength range of the bulk plasmon-polariton modes were studied (Figure 2a,b). The contribution of all optical modes available for the emitters to decay was measured, collecting all the emission angles up to the numerical aperture of the objective used (see Methods section). While for the emitters in a polymer film on glass, monoexponential decays of the fluorescence is observed, for emitters placed inside metamaterials, the PL decay is more complex (Figure 4a,c). This is consistent with a distance and polarization dependent distribution of the emitters within the metamaterial with respect to the nanorods, leading to a distribution of the spontaneous decay rates[13] and, thus, multiexponential decays of the observed PL. In order to analyze the decay properties, an inverse Laplace transform-based analysis was performed to extract the distribution of the lifetimes without any initial assumptions[30] (See Methods section).

While the different dyes exhibit fluorescence lifetimes comprised between 2 and 3 ns when embedded in a uniform polymer matrix (Figure 4a,b), strongly modified decay rates have been observed for all emitters when constrained by the

metamaterial (Figure 4c,d). The lifetime distributions, determined by the emitters' positions within the metamaterial, may also be strongly influenced by its nonlocal response.[31] Indeed, such nanorod-based metamaterials support, on a microscopic level beyond the effective medium approximation, cylindrical surface plasmons close to the emission wavelengths of the dyes in both the elliptic and hyperbolic regime.[32,33] In this case, emitters placed in the nanorod vicinity will experience a strong enhancement of spontaneous emission,[13] as observed in Figure 5.

For the emitters in the metamaterial environment, two distinct families of lifetimes are observed (Figure 4d), one corresponding to the lifetime reduction of 2−3× and the other with a broad distribution that corresponds to the strongest decay rate reduction by almost 50× (Figure 5b). By comparing the experimental results to numerical simulations, these two families of lifetimes can be ascribed to the emitters situated in a polymer layer above the metamaterial (weak decay rate modification) and within the metamaterial (strong decay rate modification). Numerical modeling confirms a strong position dependence of the spontaneous emission rate with respect to the nanorod in both lateral direction (xy-directions) as well as with respect to the surface of the metamaterial waveguide (z-direction). This is illustrated by the simulated power flow along the waveguide for the emitters at different positions within the waveguide. In particular, the efficient coupling to the TM1 mode, observed experimentally (Figure 3a,b), is confirmed by the simulations (Figure 5d). In a good correspondence between simulations and experiment, the TM mode is narrower and TE mode is much broader. As expected, the most efficient coupling to TE and TM modes is achieved for emitters at different
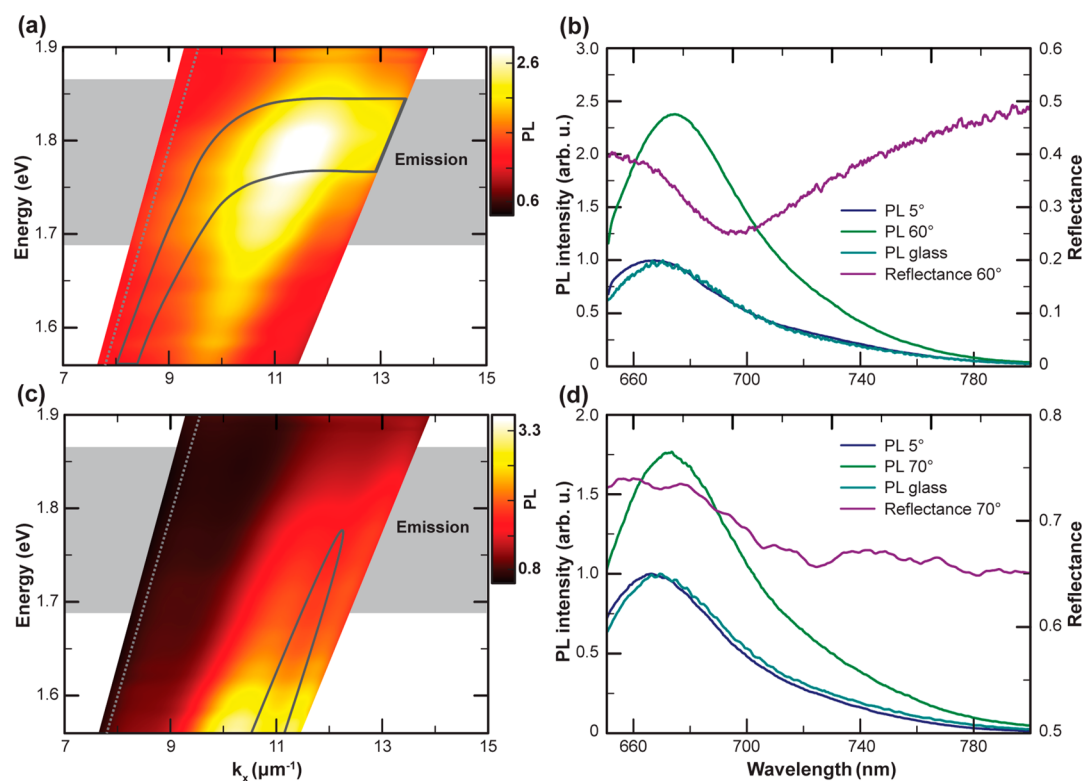
Figure 3. Emission in waveguided modes. (a, c) Experimental dispersions of the photoluminescence (PL) enhancement measured for (a) TM- and (c) TE-polarized emission. The PL spectra are normalized to the PL spectrum near the normal detection (5°). The position of the TM and TE modes, reproduced from the reflection dispersion in Figure 2a,c, are added as a guide to the eye. The position of the light line in air (gray dotted line), the emission band of LD700 dye (greyed region) are shown. (b, d) Spectra of the photoluminescence measured for (b) TM and (d) TE polarized emitted light for the LD700-doped polymer on a glass substrate and in the metamaterial at the angle of detection of 5°, 60°, and 70° and the corresponding reflectance spectra. The PL spectra on glass and near the normal detection are normalized to 1, the PL spectra at higher angles of detection are normalized to the maximum intensity measured at 5°.

positions in the metamaterial slab as it strongly depends on the emitter position with respect to both the mode profile and the nanorods (Figure 5c,d).

The fluorescence processes inside the nanostructured composite have a complex nature. Emitters situated inside metamaterials are always influenced by the near-field of adjacent nanorods where the electromagnetic field is dominated by high-wavevector components.[16] In this case, a conventional EMT theory, which does not account for internal local fields, is not applicable, and the interaction of the near-field with the exact nanorod geometry needs to be considered. It should be noted, however, that the extension of EMT to take into account the nonlocal effects, allows a partial description of local plasmonic fields and thus related fluorescence processes.[31,32] At certain wavelengths, this near-field-mediated emission may then be coupled to a set of the metamaterial slab modes.[13,29] These modes can be adequately described both by the EMT and in the microscopic model of the nanorod composite and explain the fluorescence evolution in the far-field of the emitter and its outcoupling to free-space.

The transition dipole moments of the dye molecules dispersed in PMMA have random orientations. Hence, they can emit into both TM and TE modes of the metamaterial slab and subsequently outcoupled in free space beyond the metamaterial. The emission efficiency in each particular mode depends on the emitter position with respect to the adjacent nanorods, dipole moment orientation and the field distribution of the slab modes (particularly, the metamaterial Fabry−Perot

or waveguided modes) at the emission frequency. The numerical modeling indicates that dipoles oriented along the nanorods emit mostly in TM-polarized modes, while dipoles oriented perpendicularly to the nanorods can couple to both TM and TE modes. Thus, for an arbitrary-oriented dipole the ratio between the emission in modes with TM and TE polarizations will be defined, in part, by the angle between the dipole and the nanorod axis.

The role of the availability of the slab modes can be clearly seen in the experimental results (Figure 3a,c): at lower frequencies, the emission into the metamaterial slab is dominated by the TE-polarized mode, while at ~1.8 eV (corresponding to the wavelength of 700 nm), the TM mode starts to play an essential role. The same can be observed in the numerical results (Figure 5c,d). The coupling to the TM mode is efficient only for the dipole located at the quarter-rod height due to the field overlap with the available waveguided mode strongly localized near the metamaterial-substrate interface (right panel of Figure 5a), while the TE mode profile extends across the metamaterial slab and the ratio of the intensity coupling efficiencies for the emitters at the quarter- and half-height positions of the unit cell is about 2, in agreement with the modal profile (Figure 5a). The difference in the experimentally observed coupling efficiencies in the TE and TM modes (Figure 3b,d) are in good agreement with the model estimations.

The free space emission following outcoupling of the modes in the substrate and superstrate, integrated over all angles in
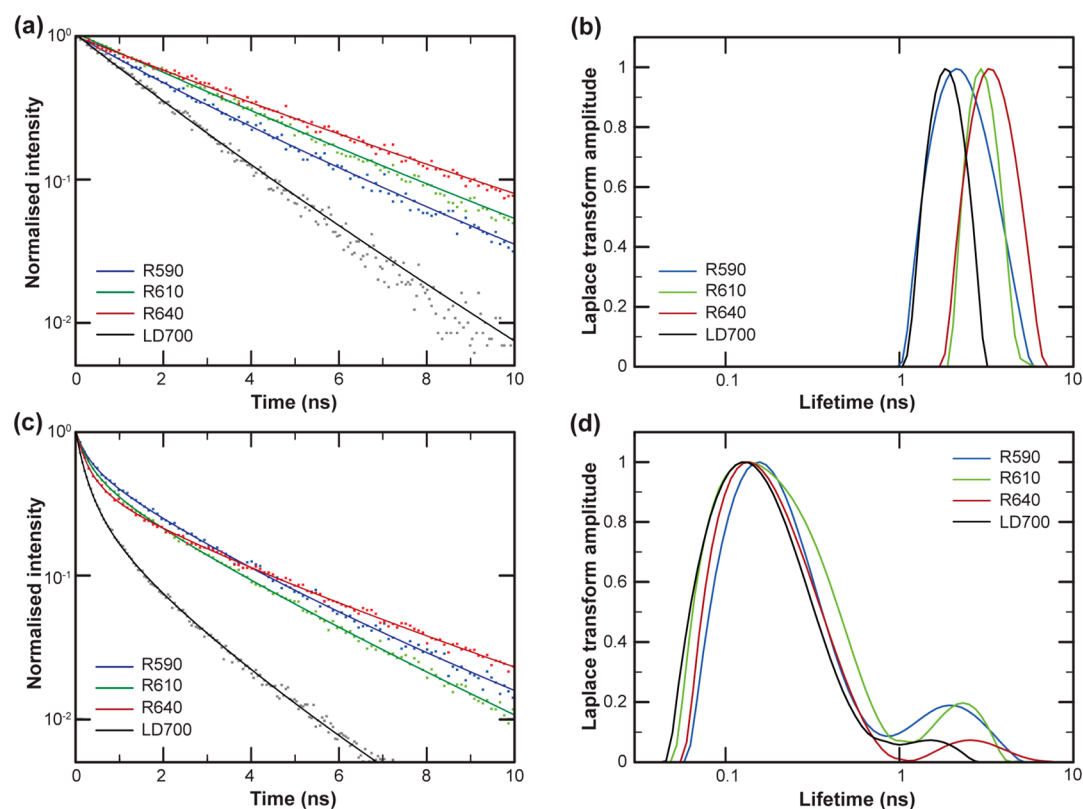
Figure 4. Time-resolved photoluminescence decays and inverse Laplace transform data analysis. (a, c) Dynamics of the fluorescence decay of the emitters in a dye-doped PMMA layer (a) on a glass substrate and (c) inside the metamaterial. (b, d) Experimental fluorescence lifetime distributions of the emitters (b) on a glass substrate and (d) inside the metamaterial extracted using an inverse Laplace transform method from the time-resolved PL measurements.

glass and in PMMA, amounts to 5−16% of the intensity emitted by the dipole in the slab. For example, for the wavelength of 670 nm, 8% of the total emission is outcoupled in the superstrate and 5% in the substrate for the dipole in the center of the unit cell (purple dipole in left panel of Figure 5a). The remaining energy is coupled to the metamaterial modes and eventually dissipated. At the same time for dipoles diagonally located inside the metamaterial (green dipole in left panel of Figure 5a), the outcoupling efficiency to free space is only 1−6%, depending on the emission wavelength, as the quenching is higher for these emitter positions, since they are located closer to the nanorods.

Similarly, for the emitters outside, but in the near-field proximity of the metamaterial slab (dark blue dipole in left panel of Figure 5a), free-space radiation accounts for 10−18% of the total radiation depending on the wavelength, with, for a wavelength of 670 nm, 8% of the total emission directed in the superstrate and 7% in the substrate primarily via the metamaterial mode. The rest of the emission is coupled to truly waveguided metamaterial modes which are not coupled to the superstrate and dissipated. For emitters situated above individual rods (light blue dipole in left panel of Figure 5a), the coupling to free-space radiation corresponds to 4−10% depending on the wavelength; for example, at a wavelength of 670 nm, 4% is emitted in the superstrate where the emitters are located and 3% in the substrate. Therefore, the far-field emission efficiency is not strongly dependent upon whether emitters are place inside or outside the metamaterial since the high density of optical states ensures significant emission radiation in the waveguided metamaterial modes.

These observations also confirm that the mode structure of the metamaterial layer or resonators may have a more significant role in defining the waveguided or free-space emission intensity, while the decay rate enhancement effect is, to a large extent, determined by the local fields near the nanorods.[26] Thus, despite the high Purcell factor observed for certain emitters' locations, the overall emission intensity enhancement is moderate, due to the averaging over all the positions of the emitters inside the metamaterial. Nevertheless, in the experiments with precisely positioned single emitters, both strong reduction of the lifetime and increase of the total emitted intensity should be pronounced.

The survey of the experimental results on spontaneous emission control using hyperbolic metamaterials show that the emitters placed on top of a metal-dielectric multilayer or a nanorod-based metamaterial generally exhibit moderate enhancement of decay rates up to 6-[21] and 9-fold,[18] respectively, comparable to the results of the present work (up to 3-fold). In the case of nanopatterned multilayer metamaterials, allowing the emitters to be located "inside" the metamaterial and an optimized out-coupling of the emission to the far-field, strong enhancements of the decay rate and quantum efficiency of up to 76 and 80 times, respectively, have been reported.[19] Hyperbolic nanorod metamaterials, however, have the advantage of exhibiting broadband enhancement of decay rates, achievable over large surface areas thanks to their fabrication process. In the nanorod metamaterial, the ultimate limit of the lifetime shortening is defined by the practical cutoff of the available modes with large wavevectors associated with cylindrical surface plasmons of the nanorods and their
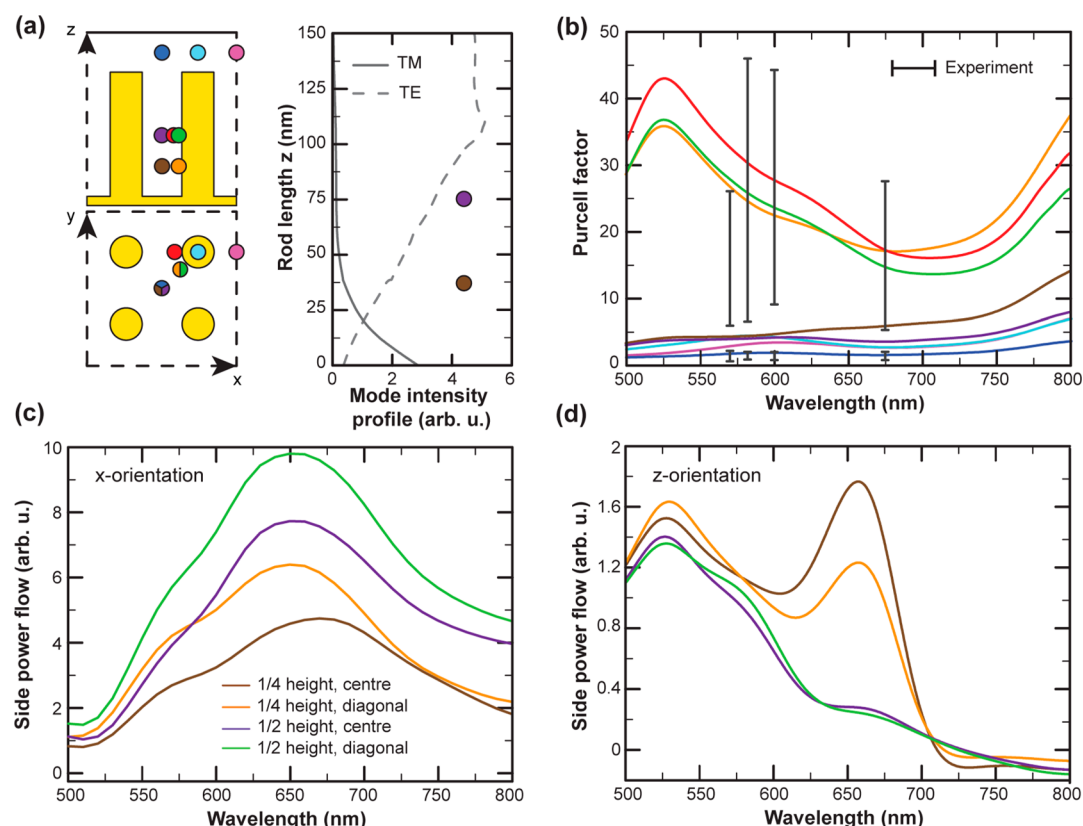
Figure 5. Numerical simulations. (a) Left panel: Side and top views of a 4 × 4 nanorod array section. The eight colored dots represent the different positions of the dipoles considered in the finite element method modeling. Right panel: simulated mode intensity profiles of TE-polarized ($|E_x|^2$) and TM-polarized ($|E_z|^2$) modes propagating in the y-direction. (b) Spectral dependence of the lifetime averaged over the dipole orientation for different locations of the dipoles represented in (a). The black vertical bars correspond to the experimental data related to the width of the lifetime distribution at 50% of the modal amplitude for both peaks ([Figure 4](#)d). (c, d) Power flow along the metamaterial waveguide for different locations of a dipole oriented in (c) x- and (d) z-direction (color coding as in (c)).

interaction as well as material losses.[31] Smaller separations and lower losses would allow higher-wavevector modes accepted by the metamaterial composite, and the practical limit is defined by the available fabrication methods. Other factors limiting the lifetime shortening are related to the emitters' positioning[31] and their non-negligible size.[24]

Effective quantum yield is another important consideration for spontaneous emission engineering in addition to the decay rate. Various plasmonic nanoantennas provide modest rate enhancements with reasonably good quantum yield but the emission is radiated in free space. For practical, integrated optics applications, the coupling to waveguided modes is beneficial, which can be achieved with the proposed approach. The propagation lengths of the TM hyperbolic waveguided modes in a plasmonic metamaterial are quite small due to the strong field confinement and are on the order of a few μm depending on the wavelength, as estimated from numerical simulations, which corresponds to few 100s of nanorods. However, such metamaterial waveguides can be seamlessly integrated in low-loss (e.g., Si-based) waveguides[34] for achieving bright and fast light sources provided by high Purcell enhancement. The interplay between the emission rate increase, the quantum yield (influenced by nonradiative quenching), and coupling to a required waveguided mode strongly depends on the position of the emitters with respect to the nanorod forming the metamaterial as was shown in ref [31] and in this work.

CONCLUSION

We have investigated spontaneous emission inside a hyperbolic metamaterial slab and showed the role of the waveguided modes of the metamaterial layer in this process. A very strong, almost 50-fold, acceleration of the spontaneous decay has been observed for emitters inside the metamaterial slab, which is strongly position dependent. At the same time, only a weak rate modification (several times) was observed for emitters in the proximity of the metamaterial waveguide interface. In both cases, up to approximately 18% of radiation, depending on the emitter position with respect to the nanorods, is coupled to far-field radiation in the substrate and the superstrate, with the remaining energy coupled to the true waveguided modes of the slab. The emission spectrum is also significantly modified due to the coupling to waveguided modes and is different for different emission polarizations. These results demonstrate the capability of such active hyperbolic metamaterials to exhibit highly tunable electromagnetic properties for the design of integratable, enhanced and fast light sources for various nanophotonic components, with the potential to enable the creation of highly integrated single-photon sources. The emission coupled to a metamaterial waveguide can be accessed by incorporating a metamaterial slab in or onto dielectric photonic waveguides, including Si photonic circuitry. Spontaneous emission modification inside hyperbolic metamaterial waveguides can also be implemented in other systems, such as metal-dielectric multilayers or natural hyperbolic materials,

potentially allowing a more controllable positioning of the emitters inside the waveguide.

■ METHODS

Fabrication of Metamaterial and Dye Deposition. The metamaterials were fabricated following the protocol described in ref 28 by electrodepositing Au into a porous anodized aluminum oxide (AAO) matrix, which was subsequently removed. The metamaterials parameters were approximately 38 nm rod diameter, 80 nm rod spacing and 150 nm rod length. The dye-doped PMMA layer with a doping concentration of 1.5 wt % was then spin-coated onto the metamaterial. To probe the Purcell effect in both the elliptical and hyperbolic regimes of the metamaterial dispersion, four identical metamaterial samples were used to deposit four laser dyes (Rhodamine perchlorate dyes) with different emission wavelengths distributed over a wide range of the visible spectrum: Rhodamine 590 (R590), Rhodamine 610 (R610), Rhodamine 640 (R640), and Rhodamine 700 (LD700). The presence of the polymer (PMMA) matrix results in a blue-shifted ENZ wavelength compared to the nanorods in AAO matrix (Figure 1c) as $n_{\text{PMMA}} < n_{\text{AAO}}$.

Optical Characterization. Angle-resolved transmission and reflection spectroscopy was performed using light from a tungsten-halogen lamp polarized and collimated onto the sample from the substrate side and then collected by an objective lens and coupled to a spectrometer equipped with a CCD camera via a multimode optical fiber. In the case of attenuated total reflection (ATR) measurements for excitation or detection of the waveguided modes, the sample was placed in contact with a glass semicylinder and illuminated through it. Photoluminescence measurements were performed in ATR configuration using a 5 mW He−Ne laser excitation source. The spectral dependences of the PL intensity, for both TE and TM polarizations, were separately measured for different detection angles and then normalized to the PL spectrum near normal incidence (at an angle of 5°), revealing the influence of the coupling to the waveguided mode. The quantum yields of the four emitters where measured by a relative determination method, using the known quantum yield of R610 dye from the literature ($Q_{\text{R610}} = 0.95$). The following quantum yields were then obtained for the other emitters: 0.54 for R590, 0.76 for R640, and 0.25 for LD700.

Time-Resolved Photoluminescence Measurements. Time-resolved photoluminescence analysis was performed using time-correlated single photon counting technique (TCSPC) equipped with SPC-150 (Becker-Hickl). TM-polarized excitation light (532 nm for R590/R610/R640 and 633 nm for LD700) was focused on the sample with a 4×, NA = 0.10 objective and the resulting PL collected by a high numerical aperture objective (90×, NA = 0.90), within a 64° angle range, corresponding to the numerical aperture of the objective. Different filters were used to remove the laser contribution to the measured light. Time-resolved PL decays of the emitters were measured inside the metamaterial and in a polymer matrix for reference.

Fluorescence Lifetime Data Analysis. Time-resolved PL decays were analyzed using an inverse Laplace transform method[30] in order to extract the lifetime distributions of the emitters inside the metamaterial as well as in the polymer matrix. This method, which does not require any initial estimation of the lifetime distribution, is based on the solution of the equation

$$I(t) = \int_0^{\infty} F(\tau)e^{-t/\tau}\,\mathrm{d}\tau \tag{1}$$

where $I(t)$ is the measured time-resolved PL decay deconvoluted from the instrumental response function and $F(\tau)$ is the relative weight of the exponential decay components. Due to the ill-defined characters of such inverse methods, an iterative fitting procedure was adopted to obtain stable results.

EMT Modeling. The optical properties of the metamaterial were modeled using the Maxwell-Garnet type local effective medium theory (EMT) which can be validated through the comparison with the experimental results and microscopic numerical modeling.[35] The in-plane (*xy*-directions) and out of plane (*z*-direction) components of the effective dielectric permittivity are expressed as $\epsilon_{xy}^{\text{eff}} = \epsilon_{\text{h}} \frac{(1+p)\epsilon_{\text{Au}} + (1-p)\epsilon_{\text{h}}}{(1-p)\epsilon_{\text{Au}} + (1+p)\epsilon_{\text{h}}}$ and $\epsilon_z^{\text{eff}} = p\epsilon_{\text{Au}} + (1-p)\epsilon_{\text{h}}$, respectively, where $p = \mu(r/d)^2$ is the nanorod concentration with r being the radius of the nanorods and d being the distance between the nanorods, ϵ_{Au} and ϵ_{h} are the permittivities of gold (values are taken from ref 36 with the corrections for the restricted path $R = 5$ nm as in ref 37) and the host medium, respectively. The same permittivities were used in the numerical modeling. This EMT model is valid away from the Brillouin zone edge of the nanorod array. The effective bulk plasma frequency of Au nanorod metamaterials is determined by $\text{Re}(\epsilon_z) = 0,$[29] separating the elliptic dispersion regime, where the metamaterial behaves as a strongly anisotropic dielectric, and the hyperbolic regime where the metamaterial can support bulk plasmon-polaritons due to its metallic and dielectric behavior at the same wavelength but different polarizations of light. The modes of the planar waveguides were simulated via the transfer matrix method approach,[29] taking into account the exact structure of the sample with a 10 nm Au underlayer and a 50 nm PMMA overlayer. It should be noted that while the local EMT can reasonably well predict far-field linear optical properties of a nanorod metamaterial[37] and waveguided modes[38] for not too low losses, the Purcell effect can be significantly influenced by the nonlocal response of the composite.[31] We used the EMT to describe only the waveguided mode structure. The full-vectorial numerical modeling was used for the simulations of spontaneous emission properties which depend on the local fields, not described by the local EMT. The nonlocal corrections for the waveguided modes considered in this work is estimated from comparison between the EMT and numerical simulations to be of the order of a few percent.

Numerical Modeling. A finite element method (FEM, Comsol Multiphysics software) was employed for the numerical simulations of a dye molecule emission inside or in the vicinity of the nanorod array. The Purcell factor was determined as a ratio of power flow flux from a point dipole (emulating the dye emitter) placed at a given position inside or outside the metamaterial to the corresponding power flow for a dipole in uniform PMMA.[39] The Purcell factor and the emission into metamaterial modes were found to be significantly dependent on the dipole position and orientation, which is shown by the color-coding of the lines and orientation labels in Figure 5. Two methods were used for the calculation of the power flow flux $F(\mathbf{r})$: (1) the integration of the Poynting vector over a surface of a small sphere of a 5 nm radius enclosing the point dipole and (2) through the dipole energy dissipation rate $W(r) = -1/2\text{Re}\{J^*\cdot E(r)\}$, where $E(r)$ is the

electric field of the dipole at the point of its location and J is the dipole current. The results from both methods were found to be in excellent agreement. To take into account that the emitting dipole is arbitrarily oriented, the power flow flux was calculated separately for dipoles directed along each of the coordinate axes, and the averaged value was calculated as $F(\mathbf{r}) = 1/3 \cdot F_x(\mathbf{r}) + 1/3 \cdot F_y(\mathbf{r}) + 1/3 \cdot F_z(\mathbf{r})$.[40] In order to simulate an infinite nanorod array, finite-size square arrays were modeled with their sizes gradually increased, while the convergence of the results was monitored. The simulation domain was surrounded by a set of perfectly matched layers ensuring the absence of reflections form the outer boundaries. The observed results revealed that a 10×10 nanorod array can be used to analyze the dye emission in an infinite metamaterial slab.

■ AUTHOR INFORMATION

Corresponding Author

*E-mail: diane.roth@kcl.ac.uk.

ORCID ⊙

Diane J. Roth: 0000-0002-6733-6663

Antony Murphy: 0000-0003-4039-9063

Stéphane Kéna-Cohen: 0000-0001-5065-2750

Present Address

∥Department of Physics, University of North Florida, U.S.A.

Author Contributions

The manuscript was written through contributions of all authors. All authors have given approval to the final version of the manuscript.

Notes

The authors declare no competing financial interest.

■ REFERENCES

(1) Purcell, E. M. Spontaneous emission probabilities at radio frequencies. *Phys. Rev.* **1946**, *69*, 681–681.

(2) Fussell, D.; McPhedran, R.; De Sterke, C. M. Three-dimensional Green's tensor, local density of states, and spontaneous emission in finite two-dimensional photonic crystals composed of cylinders. *Phys. Rev. E* **2004**, *70*, 066608.

(3) Novotny, L.; Hecht, B. *Principles of Nano-Optics*; Cambridge University Press, 2012.

(4) Lodahl, P.; van Driel, A. F.; Nikolaev, I. S.; Irman, A.; Overgaag, K.; Vanmaekelbergh, D.; Vos, W. L. Controlling the dynamics of spontaneous emission from quantum dots by photonic crystals. *Nature* **2004**, *430*, 654–657.

(5) Birowosuto, M. D.; Sumikura, H.; Matsuo, S.; Taniyama, H.; van Veldhoven, P. J.; Notzel, R.; Notomi, M. Fast Purcell-enhanced single photon source in 1550 nm telecom band from a resonant quantum dot-cavity coupling. *Sci. Rep.* **2012**, *2*, 321.

(6) Reithmaier, J. P.; Sek, G.; Loffler, A.; Hofmann, C.; Kuhn, S.; Reitzenstein, S.; Keldysh, L. V.; Kulakovskii, V. D.; Reinecke, T. L.; Forchel, A. Strong coupling in a single quantum dot-semiconductor microcavity system. *Nature* **2004**, *432*, 197–200.

(7) Intallura, P. M.; Ward, M. B.; Karimov, O. Z.; Yuan, Z. L.; See, P.; Shields, A. J.; Atkinson, P.; Ritchie, D. A. Quantum key distribution using a triggered quantum dot source emitting near 1.3 mu m. *Appl. Phys. Lett.* **2007**, *91*, 161103.

(8) Tam, F.; Goodrich, G. P.; Johnson, B. R.; Halas, N. J. Plasmonic enhancement of molecular fluorescence. *Nano Lett.* **2007**, *7*, 496–501.

(9) Goffard, J.; Gérard, D.; Miska, P.; Baudrion, A.-L.; Deturche, R.; Plain, J. Plasmonic engineering of spontaneous emission from silicon nanocrystals. *Sci. Rep.* **2013**, *3*, 2672.

(10) Bermúdez-Ureña, E.; Gonzalez-Ballestero, C.; Geiselmann, M.; Marty, R.; Radko, I. P.; Holmgaard, T.; Alaverdyan, Y.; Moreno, E.; García-Vidal, F. J.; Bozhevolnyi, S. I.; Quidant, R. Coupling of individual quantum emitters to channel plasmons. *Nat. Commun.* **2015**, *6*, 7883.

(11) Poddubny, A.; Iorsh, I.; Belov, P.; Kivshar, Y. Hyperbolic metamaterials. *Nat. Photonics* **2013**, *7*, 948–957.

(12) Ferrari, L.; Wu, C.; Lepage, D.; Zhang, X.; Liu, Z. Hyperbolic metamaterials and their applications. *Prog. Quantum Electron.* **2015**, *40*, 1–40.

(13) Poddubny, A. N.; Belov, P. A.; Ginzburg, P.; Zayats, A. V.; Kivshar, Y. S. Microscopic model of Purcell enhancement in hyperbolic metamaterials. *Phys. Rev. B: Condens. Matter Mater. Phys.* **2012**, *86*, 035148.

(14) Krishnamoorthy, H. N. S.; Jacob, Z.; Narimanov, E.; Kretzschmar, I.; Menon, V. M. Topological transitions in metamaterials. *Science* **2012**, *336*, 205–209.

(15) Kabashin, A. V.; Evans, P.; Pastkovsky, S.; Hendren, W.; Wurtz, G. A.; Atkinson, R.; Pollard, R.; Podolskiy, V. A.; Zayats, A. V. Plasmonic nanorod metamaterials for biosensing. *Nat. Mater.* **2009**, *8*, 867–871.

(16) Tsai, K.-T.; Wurtz, G. A.; Chu, J.-Y.; Cheng, T.-Y.; Wang, H.-H.; Krasavin, A. V.; He, J.-H.; Wells, B. M.; Podolskiy, V. A.; Wang, J.-K. Looking into meta-atoms of plasmonic nanowire metamaterial. *Nano Lett.* **2014**, *14*, 4971–4976.

(17) Caldwell, J. D.; Kretinin, A. V.; Chen, Y.; Giannini, V.; Fogler, M. M.; Francescato, Y.; Ellis, C. T.; Tischler, J. G.; Woods, C. R.; Giles, A. J.; Hong, M.; Watanabe, K.; Taniguchi, T.; Maier, S. A.; Novoselov, K. S. Sub-diffractional volume-confined polaritons in the natural hyperbolic material hexagonal boron nitride. *Nat. Commun.* **2014**, *5*, 5221.

(18) Kim, J.; Drachev, V. P.; Jacob, Z.; Naik, G. V.; Boltasseva, A.; Narimanov, E. E.; Shalaev, V. M. Improving the radiative decay rate for dye molecules with hyperbolic metamaterials. *Opt. Express* **2012**, *20*, 8100–8116.

(19) Lu, D.; Kan, J. J.; Fullerton, E. E.; Liu, Z. W. Enhancing spontaneous emission rates of molecules using nanopatterned multilayer hyperbolic metamaterials. *Nat. Nanotechnol.* **2014**, *9*, 48–53.

(20) Gu, L.; Tumkur, T.; Zhu, G.; Noginov, M. A. Blue shift of spontaneous emission in hyperbolic metamaterial. *Sci. Rep.* **2015**, *4*, 4969.

(21) Shalaginov, M. Y.; Vorobyov, V. V.; Liu, J.; Ferrera, M.; Akimov, A. V.; Lagutchev, A.; Smolyaninov, A. N.; Klimov, V. V.; Irudayaraj, J.; Kildishev, A. V. Enhancement of single-photon emission from nitrogen-vacancy centers with TiN/(Al, Sc)N hyperbolic metamaterial. *Laser Photonics Rev.* **2015**, *9*, 120–127.

(22) Noginov, M. A.; Li, H.; Barnakov, Y. A.; Dryden, D.; Nataraj, G.; Zhu, G.; Bonner, C. E.; Mayy, M.; Jacob, Z.; Narimanov, E. E. Controlling spontaneous emission with metamaterials. *Opt. Lett.* **2010**, *35*, 1863–1865.

(23) Jacob, Z.; Smolyaninov, I. I.; Narimanov, E. E. Broadband Purcell effect: Radiative decay engineering with metamaterials. *Appl. Phys. Lett.* **2012**, *100*, 181105.

(24) Poddubny, A. N.; Belov, P. A.; Kivshar, Y. S. Spontaneous radiation of a finite-size dipole emitter in hyperbolic media. *Phys. Rev. A: At., Mol., Opt. Phys.* **2011**, *84*, 023807.

(25) Ferrari, L.; Lu, D. L.; Lepage, D.; Liu, Z. W. Enhanced spontaneous emission inside hyperbolic metamaterials. *Opt. Express* **2014**, *22*, 4301–4306.

(26) Slobozhanyuk, A. P.; Ginzburg, P.; Powell, D. A.; Iorsh, I.; Shalin, A. S.; Segovia, P.; Krasavin, A. V.; Wurtz, G. A.; Podolskiy, V.

A.; Belov, P. A.; Zayats, A. V. Purcell effect in hyperbolic metamaterial resonators. *Phys. Rev. B: Condens. Matter Mater. Phys.* **2015**, *92*, 195127.

(27) Ginzburg, P.; Krasavin, A. V.; Poddubny, A. N.; Belov, P. A.; Kivshar, Y. S.; Zayats, A. V. Self-induced torque in hyperbolic metamaterials. *Phys. Rev. Lett.* **2013**, *111*, 036804.

(28) Evans, P.; Hendren, W. R.; Atkinson, R.; Wurtz, G. A.; Dickson, W.; Zayats, A. V.; Pollard, R. J. Growth and properties of gold and nickel nanorods in thin film alumina. *Nanotechnology* **2006**, *17*, 5746−5753.

(29) Vasilantonakis, N.; Nasir, M. E.; Dickson, W.; Wurtz, G. A.; Zayats, A. V. Bulk plasmon-polaritons in hyperbolic nanorod metamaterial waveguides. *Laser Photonics Rev.* **2015**, *9*, 345−353.

(30) Provencher, S. W. Inverse problems in polymer characterization: direct analysis of polydispersity with photon correlation spectroscopy. *Makromol. Chem.* **1979**, *180*, 201−209.

(31) Ginzburg, P.; Roth, D. J.; Nasir, M. E.; Segovia, P.; Krasavin, A. V.; Levitt, J.; Hirvonen, L. M.; Wells, B.; Suhling, K.; Richards, D.; Podolskiy, V. A.; Zayats, A. V. Spontaneous emission in non-local materials. *Light: Sci. Appl.* **2016**, *6*, e16273.

(32) Wells, B. M.; Zayats, A. V.; Podolskiy, V. A. Nonlocal optics of plasmonic nanowire metamaterials. *Phys. Rev. B: Condens. Matter Mater. Phys.* **2014**, *89*, 035111.

(33) Podolskiy, V. A.; Ginzburg, P.; Wells, B.; Zayats, A. V. Light emission in nonlocal plasmonic metamaterials. *Faraday Discuss.* **2015**, *178*, 61−70.

(34) Neira, A. D.; Wurtz, G. A.; Ginzburg, P.; Zayats, A. V. Ultrafast all-optical modulation with hyperbolic metamaterial integrated in Si photonic circuitry. *Opt. Express* **2014**, *22*, 10987−94.

(35) Elser, J.; Wangberg, R.; Podolskiy, V. A.; Narimanov, E. E. Nanowire metamaterials with extreme optical anisotropy. *Appl. Phys. Lett.* **2006**, *89*, 261102.

(36) Johnson, P. B.; Christy, R. W. Optical constants of the noble metals. *Phys. Rev. B* **1972**, *6*, 4370.

(37) Pollard, R. J.; Murphy, A.; Hendren, W. R.; Evans, P. R.; Atkinson, R.; Wurtz, G. A.; Zayats, A. V.; Podolskiy, V. A. Optical nonlocalities and additional waves in epsilon-near-zero metamaterials. *Phys. Rev. Lett.* **2009**, *102*, 127405.

(38) Peruch, S.; Neira, A.; Wurtz, G. A.; Wells, B.; Podolskiy, V. A.; Zayats, A. V. Geometry defines ultrafast hot-carrier dynamics and Kerr nonlinearity in plasmonic metamaterial waveguides and cavities. *Adv. Opt. Mater.* **2017**, *5*, 1700299.

(39) Ford, G. W.; Weber, W. H. Electromagnetic interactions of molecules with metal surfaces. *Phys. Rep.* **1984**, *113*, 195−287.

(40) Atre, A. C.; Brenny, B. J.; Coenen, T.; Garcia-Etxarri, A.; Polman, A.; Dionne, J. A. Nanoscale optical tomography with cathodoluminescence spectroscopy. *Nat. Nanotechnol.* **2015**, *10*, 429−36.